

Model Predictive Current Control of Modular Multilevel Converters

Georgios Darivianakis, Tobias Geyer and Wim van der Merwe

ABB Corporate Research, Baden-Dättwil, Switzerland

Emails: gdarivia@student.ethz.ch, t.geyer@ieee.org, wim.van-der-merwe@ch.abb.com

Abstract—This paper proposes a model predictive controller for high-power modular multilevel converter operating at low switching frequencies. The controller regulates the load currents along their reference trajectories, controls the circulating currents and controls the sum of the capacitor voltages per branch. Upper limits on the branch currents and capacitor voltages are imposed in the controller formulation. The controller manipulates the voltage references of a carrier-based pulse width modulator. A subsequent balancing controller maintains the capacitor voltages within each branch around their average voltage. Unlike hierarchical schemes based on multiple PI control loops, the proposed controller achieves not only a very good performance at steady-state operation but also very fast current responses during load transients, while maintaining the branch currents and capacitor voltages within their safe operating limits.

I. INTRODUCTION

The modular multilevel converter (MMC) topology has lately received significant interest in the area of medium-voltage power electronics [1]. The series-connection of module capacitors allows for a scaling of the output voltages and the number of output voltage levels. Increasing the latter is beneficial from a line current total harmonic distortion (THD) point of view, since the THD can be kept within acceptable limits even when operating at very low switching frequencies. These properties make the MMC topology well suited for a variety of high-power applications, such as high-voltage direct-current (HVDC) transmission, high-power medium-voltage motor drives and static VAR compensators (STATCOM).

The control and modulation problem of the MMC is to regulate the load currents around their time-varying references, to balance the capacitor voltages around their nominal values, to minimize the converter and switching losses, and to meet harmonic requirements of the load, most notably a low current THD. The MMC must be operated within its safe operating limits, particularly with regard to the branch current and capacitor voltages. Due to the multiple-input multiple-output structure of the converter and its various internal dynamics, this control problem is intrinsically difficult to address. The vast majority of control methods proposed so far for MMCs is based on hierarchical schemes with multiple PI control loops and pulse width modulators (PWM) [2]–[5].

Hierarchical schemes with multiple PI control loops tend to perform poorly when fast dynamics during transient operation are required or when operating at low switching frequencies.

Therefore, the power electronics community has started to investigate the concept of modern control methods formulated in the time domain, most notably model predictive control (MPC) [6]. According to the MPC philosophy, a performance index is minimized subject to the evolution of a dynamical model over a finite-time horizon and constraints on the manipulated variables, states and outputs. The use of a discrete-time state-space model allows MPC to predict the future behavior of the plant and to optimize its control actions accordingly [7]. The literature on MPC schemes for the MMC topology is scarce and restricted to direct MPC methods that do not use a modulator [8]–[11].

This paper proposes a PWM-based model predictive current controller (MPCC) for the MMC. It appears to be the first MPC scheme in the literature that uses a PWM. A prediction horizon of five to 10 steps is used. The underlying optimization problem is a quadratic program (QP), which can be solved efficiently using off-the-shelf solvers. The control problem is formulated in a hierarchical manner. The MPCC scheme constitutes the upper layer; it provides voltage references to the subsequent PWM and the balancing control algorithm on the lower layer.

The MPCC scheme provides optimal control actions both at steady-state operation as well as during transients, such as power up, load steps and faults. Due to the ability of MPC to address constraints, the proposed controller achieves fast transient responses while respecting the imposed constraints on the branch currents and capacitor voltages, thus ensuring that the converter operates under safe conditions even during transient operation. This stands in stark contrast to the traditionally used hierarchical controllers with multiple PI loops, see e.g. [3].

The proposed MPCC scheme is formulated independently of the number of modules per branch. The use of a PWM modulator ensures an effectively constant switching frequency and a clearly defined harmonic spectrum of the load currents. These features along with the low device switching frequency of a few 100 Hz that the MPC scheme can operate at, make the developed framework suitable for high-power MMC applications.

II. PHYSICAL MODEL OF THE MMC

A. Topology

The investigated MMC topology is shown in Fig. 1. Each phase leg $p \in \{a, b, c\}$ of the converter is divided into two

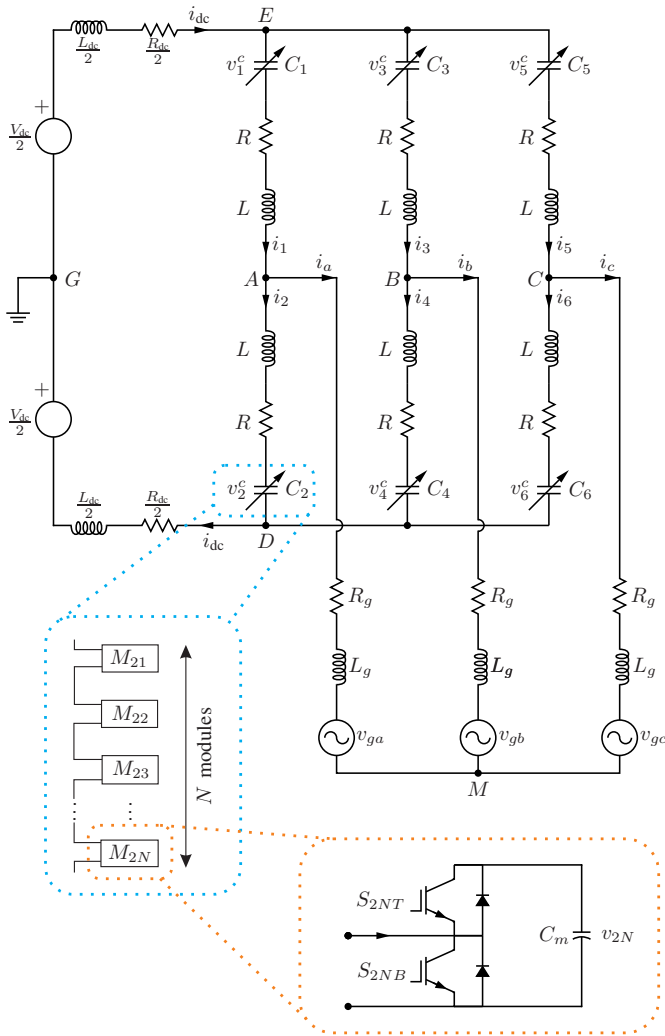


Fig. 1. Three-phase dc-ac MMC topology with unidirectional modules

branches. Each branch $r \in \{1, \dots, 6\}$ consists of N modules M_{rj} , with $j \in \{1, \dots, N\}$, and the branch inductor L . The conduction losses of each branch are modeled by the resistor R .

Each module consists of the capacitor C_m with the voltage v_{rj} and two IGBTs that form a half bridge. The IGBTs are driven by the gating signals S_{rjB} and S_{rjT} , which refer to the bottom and the top IGBT of the j th module in the r th branch. The switching behaviour of the module M_{rj} can be described using two states: (a) the on-state (i.e. $S_{rjT} = \text{on}$ and $S_{rjB} = \text{off}$), in which the capacitor C_m is connected to the branch and the terminal voltage of the module is v_{rj} , and (b) the off-state (i.e. $S_{rjT} = \text{off}$ and $S_{rjB} = \text{on}$), in which the module is bypassed.

The inductor L_{dc} and the resistor R_{dc} are connected in series to the dc supply voltage V_{dc} , which model the parasitic inductance and resistance, respectively. The three-phase output terminals of the MMC are connected to the load, which consists of the load inductor L_g in series with the load resistor

R_g and the grid voltage v_{gp} .

B. Modeling of the MMC

For each branch r we define the insertion index $n_r \in \{0, \frac{1}{N}, \frac{2}{N}, \dots, 1\}$, where $n_r = 1$ means that all N modules in the branch are inserted and $n_r = 0$ that all N modules in the branch are bypassed [2]. When assuming that all modules have the same capacitance and that the capacitor voltages are balanced [12], the series-connection of the modules inserted in branch r can be described by the (time-varying) branch capacitance

$$C_r = \frac{1}{n_r} \frac{C_m}{N} \quad (1)$$

with the voltage

$$v_r^c = n_r v_r^\Sigma. \quad (2)$$

The second term in (2) is the sum of all capacitor voltages of branch r (regardless of whether the module is inserted into the branch or not), which is defined as

$$v_r^\Sigma = \sum_{j=1}^N v_{rj}. \quad (3)$$

Moreover, the evolution of v_r^Σ is a function of the branch current i_r and the inserted branch capacitance C_r , i.e.

$$\frac{dv_r^\Sigma}{dt} = \frac{i_r}{C_r} = \frac{N}{C_m} n_r i_r, \quad (4)$$

For a sufficiently large number of modules and/or a high switching frequency, the insertion index n_r can be considered to be a real-valued variable $n_r \in [0, 1]$. This allows the derivation of a nonlinear continuous-time dynamical model of the MMC with real-valued variables. The inputs to the system are the insertion indices n_r of the six branches $r \in \{1, \dots, 6\}$. Since there are five linearly independent currents, we choose as state variables the branch currents of phase legs a and b (i.e. i_r with $r \in \{1, \dots, 4\}$), the dc-link current i_{dc} , the sums of the capacitor voltages v_r^Σ of the six branches $r \in \{1, \dots, 6\}$ and the grid voltages $v_{g\alpha}, v_{g\beta}$ in the orthogonal $\alpha\beta$ coordinate system. The outputs of the model are the load currents i_α, i_β in the orthogonal coordinate system, along with the six sums of capacitor voltages per branch v_r^Σ .

The state-space equations of the five independent currents can be easily derived by applying Kirchoff's voltage law to the five circuit meshes EADGE, EBDGE, ECDGE, DAMBD and DAMCD. The differential equations of the sum of capacitor voltages per branch v_r^Σ are given by (4). The evolution of the grid voltages in the $\alpha\beta$ frame is given by

$$\frac{d}{dt} \begin{bmatrix} v_{g\alpha} \\ v_{g\beta} \end{bmatrix} = \omega \begin{bmatrix} 0 & -1 \\ 1 & 0 \end{bmatrix} \begin{bmatrix} v_{g\alpha} \\ v_{g\beta} \end{bmatrix}, \quad (5)$$

where $\omega = 2\pi f_0$ is the grid rotational speed, with f_0 being the electrical frequency of the grid.

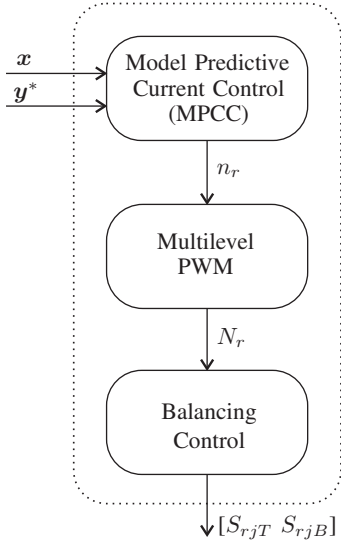


Fig. 2. Control scheme for the MMC with an upper (current) controller that manipulates the insertion index $n_r(t)$ per branch r , followed by a PWM and a lower (balancing) controller that decides on the gating signals for the IGBTs of the j th module in the r th branch

III. CURRENT CONTROL

A. Control Problem

For the MMC topology, a controller is to be developed that regulates the output load currents along their time-varying sinusoidal references, maintains the capacitor voltages close to their nominal values, and minimizes the device switching losses. Furthermore, the branch currents and the capacitor voltages are to be kept within given bounds, which are due to physical limitations of the switching devices and passive components.

The performance of the proposed controller is evaluated at steady-state operation and during transients. At steady state, the load current THD and the device switching frequency of the branch modules serve as performance metrics. During transient operation, the dynamic response of the converter is used as metric. To this end, quantities such as the overshoot, rise and settling time of a step response are examined.

B. Control Structure

To address the control problem of the MMC, a hierarchical control scheme with three levels is proposed, as depicted in Fig. 2. At the top level, an MPC scheme is devised that controls the load currents and the total energy per branch. By minimizing a quadratic cost function subject to constraints and the evolution of a linearized and real-valued state-space model of the MMC, the MPC scheme determines the optimal real-valued insertion index n_r for each of the six branches. Using (2) the insertion index n_r is translated into real-valued voltage references.

At the middle level, using a carrier-based multilevel PWM, these voltage references are translated into the six integer variables N_r , which denote the number of modules to be

inserted per branch. At the lower layer, each branch uses an independently operating controller that utilizes the redundancy within that branch to balance the capacitor voltages, by deciding on the gating commands for the individual modules.

C. Model Predictive Current Control

The MPCC scheme, as developed and implemented in this paper, is based on the principle of constrained optimal control. At each sampling instant k an optimization problem is formulated and solved in real time. The resulting sequence of control inputs $\mathbf{U} = [\mathbf{u}^T(k), \mathbf{u}^T(k+1), \dots, \mathbf{u}^T(k+N_p-1)]^T$ over the prediction horizon N_p minimizes an objective function subject to the evolution of the system model and constraints. Only the first input $\mathbf{u}(k)$ is applied to the system, and the process is repeated at the next sampling instant $k+1$ in accordance with the so called receding horizon policy [7]. The MPCC scheme is based on a linearized model of the nonlinear MMC system.

D. Linearized Prediction Model

According to the analysis in Section II, the state-space equations describing the dynamical behavior of the MMC contains the nonlinear terms $n_r v_r^\Sigma$ and $n_r i_r$. At time $t = t_0$, a first order Taylor series expansion of the above nonlinear terms around the current operating point of the system, which is given by $n_r(t_0)$, $v_r^\Sigma(t_0)$ and $i_r(t_0)$, can be performed.

$$n_r(t)v_r^\Sigma(t) = n_r(t_0)v_r^\Sigma(t) + v_r^\Sigma(t_0)\Delta n_r(t) \quad (6a)$$

$$n_r(t)i_r(t) = n_r(t_0)i_r(t) + i_r(t_0)\Delta n_r(t) \quad (6b)$$

where $\Delta n_r(t) = n_r(t) - n_r(t_0)$ is the modification in the insertion index.

The resulting linearized continuous-time prediction model is of the form:

$$\frac{d\mathbf{x}(t)}{dt} = \mathbf{A}_c(t_0)\mathbf{x}(t) + \mathbf{B}_c(t_0)\mathbf{u}(t) + \mathbf{f}_c(t_0) \quad (7a)$$

$$\mathbf{y}(t) = \mathbf{C}_c\mathbf{x}(t) \quad (7b)$$

with the state, input and output vectors

$$\mathbf{x} = [i_1 \dots i_4 \ i_{dc} \ v_1^\Sigma \dots v_6^\Sigma \ v_{g\alpha} \ v_{g\beta}]^T \quad (8a)$$

$$\mathbf{u} = [\Delta n_1 \dots \Delta n_6]^T \quad (8b)$$

$$\mathbf{y} = [i_\alpha \ i_\beta \ v_1^\Sigma \dots v_6^\Sigma]^T \quad (8c)$$

Note that $\mathbf{x} \in \mathbb{R}^{13}$, $\mathbf{u} \in [-n_1(t_0), 1 - n_1(t_0)] \times \dots \times [-n_6(t_0), 1 - n_6(t_0)] \in \mathbb{R}^6$ and $\mathbf{y} \in \mathbb{R}^8$. The time-varying matrices and vectors $\mathbf{A}_c(t_0)$, $\mathbf{B}_c(t_0)$, $\mathbf{f}_c(t_0)$ and \mathbf{C}_c are provided in the Appendix.

Using Euler's exact discretization method with the sampling interval T_s , the discrete-time representation of the linearized model can be derived.

$$\mathbf{x}(k+1) = \mathbf{A}_d(t_0)\mathbf{x}(k) + \mathbf{B}_d(t_0)\mathbf{u}(k) + \mathbf{f}_d(t_0) \quad (9)$$

E. Objective Function and Constraints

The objective function maps the control objectives into a scalar performance index. The proposed objective function consists of two parts. The first part penalizes the predicted evolution of the tracking error and the change in the manipulated variable over the prediction horizon N_p

$$\begin{aligned} J_1(\mathbf{x}(k), \mathbf{u}(k-1), \mathbf{U}) \\ = \sum_{\ell=k}^{k+N_p-1} \|\mathbf{Q}(\mathbf{y}^*(\ell) - \mathbf{y}(\ell))\|_2^2 + \lambda_u \|\mathbf{R}\Delta\mathbf{u}(\ell)\|_2^2 \end{aligned} \quad (10)$$

The matrix \mathbf{Q} penalizes the tracking error, and $\mathbf{y}^*(\ell)$ denotes the time-varying reference vector

$$\mathbf{y}^*(\ell) = [i_\alpha^*(\ell) \ i_\beta^*(\ell) \ V_{dc} \cdot \mathbb{I}_{1 \times 6}]^T. \quad (11)$$

Changes $\Delta\mathbf{u}(\ell) = \mathbf{u}(\ell) - \mathbf{u}(\ell-1)$ in the (linearized) insertion index are penalized with the matrix \mathbf{R} . Penalizing changes in the manipulated variable rather than the manipulated variable itself is preferred, since time-varying reference quantities are to be tracked. Nota that since the trade-off between tracking accuracy and control effort is determined by the ratio between \mathbf{Q} and \mathbf{R} , \mathbf{R} can be set equal to the identity matrix.

A considerable advantage of the proposed control framework is its ability to address constraints during the controller synthesis. These constraints result from the operation principles of the converter, and can be categorized either as hard or soft constraints. Hard constraints relate to strict physical limitations of the converter, such as limits on the modulation or bounds on the safe operating range. The latter directly relate to trip levels. Hard constraints are added as inequality constraints to the optimization problem and limit the admissible state-input space. Hard constraints might lead to feasibility issues.

Soft constraints can be imposed within the admissible state-input space to restrict the operation of the MMC close to the limits of the safe operating range. Unlike hard constraints, soft constraints are added to the objective function using the notion of slack variables. A slack variable ξ maps the violation of a soft constraint into a non-negative real number, i.e. $\xi : \mathbb{R} \rightarrow \mathbb{R}_+$.

The insertion index n_r of the r th branch is limited by the hard constraint

$$0 \leq n_r(\ell) \leq 1. \quad (12)$$

As shown in Fig. 3, soft constraints on the branch current i_r can be added. Specifically, upper and lower constraints at \bar{i} and $-\bar{i}$ are introduced using the slack variable ξ_r and the three inequality constraints

$$\xi_r(\ell) \geq i_r(\ell) - \bar{i} \quad (13a)$$

$$\xi_r(\ell) \geq -(i_r(\ell) + \bar{i}) \quad (13b)$$

$$\xi_r(\ell) \geq 0. \quad (13c)$$

Similarly, an upper soft constraint at \bar{v} can be imposed on the sum of capacitor voltages per branch v_r^Σ (c.f. Fig. 4)

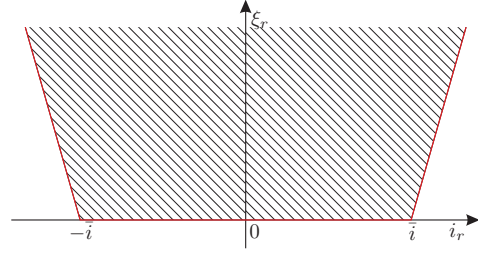


Fig. 3. Upper and lower soft constraints on the r th branch current i_r using the slack variable ξ_r .

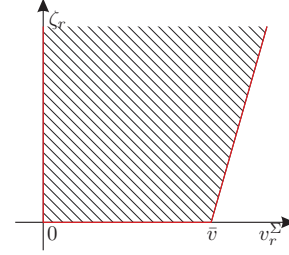


Fig. 4. Upper soft constraint on the sum of capacitor voltages v_r^Σ of the r th branch using the slack variable ζ_r .

by introducing the slack variable ζ_r and the two inequality constraints

$$\zeta_r(\ell) \geq v_r^\Sigma(\ell) - \bar{v} \quad (14a)$$

$$\zeta_r(\ell) \geq 0. \quad (14b)$$

By aggregating the slack variables in the two vectors

$$\boldsymbol{\xi} = [\xi_1 \dots \xi_6]^T \in \mathbb{R}_+^6 \quad (15a)$$

$$\boldsymbol{\zeta} = [\zeta_1 \dots \zeta_6]^T \in \mathbb{R}_+^6, \quad (15b)$$

the second part of the objective function can be written as

$$\begin{aligned} J_2(\mathbf{x}(k), \mathbf{u}(k-1), \mathbf{U}) \\ = \sum_{\ell=k}^{k+N_p-1} \lambda_\xi \|\boldsymbol{\xi}(\ell)\|_1 + \lambda_\zeta \|\boldsymbol{\zeta}(\ell)\|_1 \end{aligned} \quad (16)$$

in which the slack variables are penalized using the 1-norm and the scalar penalties λ_ξ and λ_ζ .

F. Optimization Problem

This leads to the optimization problem

$$J_{\text{opt}} = \min_{\mathbf{U}} J_1 + J_2 \quad (17)$$

subject to (9), (12), (13), (14) $\forall \ell = k, \dots, k + N_p - 1$

As the cost function is quadratic subject to the evolution of a linear state-space model with linear inequality constraints, the resulting optimization problem (17) constitutes a so-called quadratic program (QP). The QP can be formulated and solved efficiently, e.g. by using an active set method or an interior point method. The result of the optimization stage is the sequence of optimal control inputs $\mathbf{U} = [\mathbf{u}^T(k) \ \mathbf{u}^T(k+1) \ \dots \ \mathbf{u}^T(k+N_p-1)]^T$ at time step k .

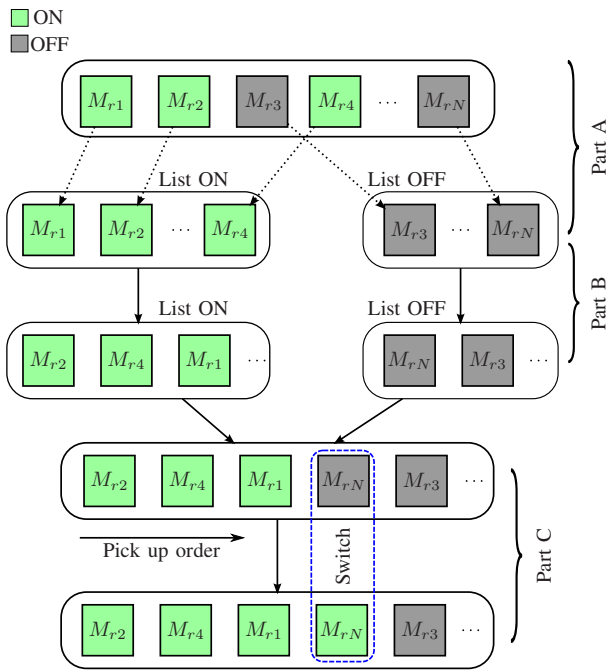


Fig. 5. Balancing controller based on two lists for branch r

The first element of the sequence of optimal control inputs is implemented at time-step k and sent to the PWM. At the next time-step $k + 1$, new measurements are obtained and the optimization problem is solved again over a shifted prediction horizon. This so called receding horizon policy provides feedback and ensures that the controller is robust to parameter uncertainties.

G. Multilevel Pulse Width Modulation

The middle level of the hierarchical control scheme (c.f. Fig. 2) executes the carrier-based PWM. The insertion index n_r can be interpreted as the modulation index of a multilevel PWM scheme, as developed and implemented in [13]. The PWM translates the real-valued reference voltage into the integer N_r , which relates to the number of modules to be inserted to the r th branch.

H. Balancing Control

The lower control layer utilizes the redundancy in the converter states to balance the capacitor voltages within the branches. Each branch uses its own balancing controller, which receives as input from the modulation stage the number of modules N_r to be inserted into the branch r . The controller computes the switching signals for the N modules, namely the gating signals S_{rjB} and S_{rjT} for the bottom and top IGBTs in the j th module.

The balancing algorithm consists of three parts. In part A, two separate and mutually exclusive lists, namely "List ON" and "List OFF", are established according to the current state of the modules in the branch. Denoting by N_{ON} and N_{OFF} the number of modules contained in "List ON" and "List OFF", respectively, it holds that $N_{ON} + N_{OFF} = N$.

| Parameter | | p.u. value | SI value |
|----------------------|----------|------------|-----------------|
| Output frequency | f_0 | 1 | 50 Hz |
| Dc supply voltage | V_{dc} | 2.1916 | 6.8 kV |
| Grid rms voltage | V_{ll} | 1.2247 | 3.8 kV |
| Load rms current | I_p | 0.7071 | 650 A |
| Capacitance | C_m | 8.6951 | 8.2 mF |
| Dc supply resistance | R_{dc} | 0.00003 | 100 $\mu\Omega$ |
| Branch resistance | R | 0.000074 | 250 $\mu\Omega$ |
| Load resistance | R_g | 0.02 | 67.5 m Ω |
| Dc supply inductance | L_{dc} | 0.0047 | 50 μ H |
| Branch inductance | L | 0.0931 | 1 mH |
| Load inductance | L_g | 0.15 | 1.6 mH |

TABLE I
MMC SYSTEM PARAMETERS

In part B, the modules of each list are sorted in an ascending or descending order of their capacitor voltage values, depending on the polarity of the respective branch current. Finally, in part C, the module selection is performed. "List ON" is always prioritized and only if $N_r > N_{ON}$ then $N_r - N_{ON}$ modules of "List OFF" are switched on. In case that $N_r \leq N_{ON}$ then $N_{ON} - N_r$ modules of "List ON" are switched off. The balancing algorithm is graphically presented in Fig. 5.

IV. PERFORMANCE EVALUATION

A. Simulation Parameters

To demonstrate the performance of the proposed MPC scheme, consider a three-phase 4.28 MVA medium-voltage MMC with $N = 8$ modules per branch, operating in dc-ac inverter mode with its input connected to a 6.8 kV dc supply. The MMC parameters are summarized in Table I. The per unit (p.u.) system is established using the base voltage $V_B = \sqrt{2/3}V_{ll} = 3.10$ kV, the base current $I_B = \sqrt{2}I_p = 919.24$ A and the base frequency $f_B = 50$ Hz.

A regularly-sampled multilevel carrier-based PWM with phase disposition is used with a carrier frequency of 2.5 kHz [14]. Consistent with the modulation scheme, for each branch, the different triangular carrier waveforms are not interleaved. A phase shift of 180 degrees is applied between the carrier waveforms of the upper and lower branches. The MMC, load, MPC scheme, PWM and balancing controller were implemented in Matlab/Simulink and PLECS.

B. MPC Settings

The MPCC scheme is executed at the peaks of the triangular carrier, i.e. every 200 μ s. The state vector \mathbf{x} is assumed to be available to the controller along with the time-varying reference signal \mathbf{y}^* . Measurement and computational delays are assumed to be fully compensated. The computed control actions are kept constant between time steps k and $k + 1$ and sent to the multilevel PWM stage.

For the objective function, the penalties

$$\mathbf{Q} = \begin{bmatrix} 10 \cdot \mathbb{I}_{2 \times 2} & \mathbf{0}_{2 \times 6} \\ \mathbf{0}_{6 \times 2} & \mathbb{I}_{6 \times 6} \end{bmatrix}, \quad \mathbf{R} = \mathbb{I}_{6 \times 6} \text{ and } \lambda_\xi = \lambda_\zeta = 10^5$$

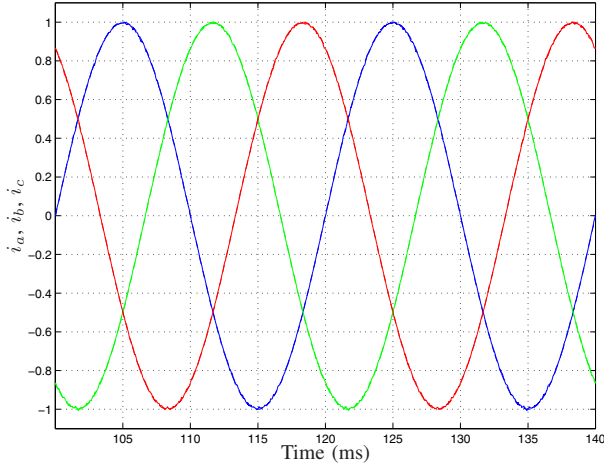


Fig. 6. Three-phase load currents at steady-state operation

are chosen. The soft constraints are activated at $\bar{i} = 1.1$ p.u. and $\bar{v} = 1.2V_{dc}$.

The choice of the prediction horizon N_p requires care. On the one hand, due to some slow dynamics in the MMC, a relatively long prediction horizon is required to ensure a good steady-state performance. On the other hand, as open-loop verification experiments show, the linearized prediction model tends to be inaccurate when predicting more than 5 ms into the future. Moreover, the computational burden of the optimization problem directly depends on the prediction horizon. Based on the above considerations, a prediction horizon of $N_p = 6$ was chosen.

The QP in (17) has at each time-step six input and 12 slack variables; for the horizon $N_p = 6$ this leads to an optimizer of dimension 108. The Multi-Parametric Toolbox 3.0 [15] and the Gurobi Optimizer [16] were used to formulate and solve the QP problem.

C. Closed Loop Evaluation

1) *Steady-State Performance:* At full load, the performance of the control scheme is evaluated at steady-state operating conditions. The three-phase load currents are shown in Fig. 6 over two fundamental periods. The MPC scheme regulates the load currents closely along their references. Over a time window of 100 ms, three performance metrics are computed. The mean square error (MSE) is $6 \cdot 10^{-5}$ p.u., the THD of the load current is 0.55%, and the average device switching frequency is 375 Hz.

The operation of the lower layer balancing algorithm can be observed in Fig. 7, which shows the voltage waveforms over two fundamental periods. The capacitor voltages are balanced within 10% of their nominal value. The visible differences in the capacitor voltages are due to the low switching frequency. The soft constraints on the total capacitor voltages along with the balancing control algorithm keep the capacitor voltages within acceptable bounds.

The soft constraints on the branch currents, which are imposed by the operational limits of the converter, are met by

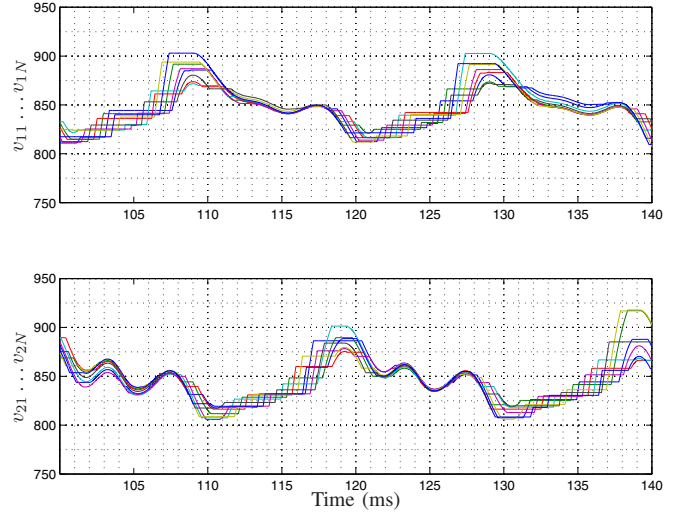


Fig. 7. Capacitor voltages of the N modules of the top and bottom branch, respectively, of the phase leg a at steady-state operation

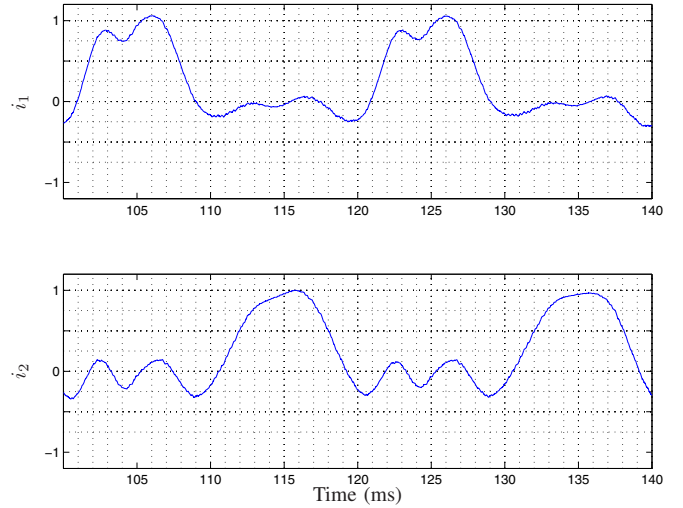


Fig. 8. Branch current of the top and bottom branch, respectively, of the phase leg a at steady-state operation

the control scheme. As shown in Fig. 8, the branch currents remain within their predefined bounds of -1.1 to 1.1 p.u.. Furthermore, by comparing the waveforms of the upper and lower branch currents of one phase leg (e.g. i_1 and i_2), we can also infer that the magnitudes of the circulating currents are small. This reduces the conduction losses in the converter.

2) *Transient Performance:* To investigate the dynamic behaviour of the system, the converter is initially operated at rated load current before the reference of the load currents is changed to zero at $t = 110$ ms. At $t = 130$ ms, the load current reference is changed back to 1 p.u.. The resulting dynamic response of the three-phase load current is shown in Fig. 9. The MPCC scheme achieves very fast current responses without overshoots. For the negative step, when sufficient voltage margin is available, the current transient requires about

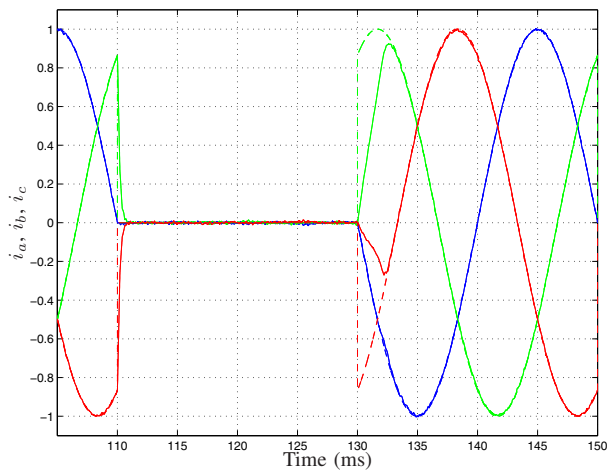


Fig. 9. Three-phase load currents and their dashed references during load steps

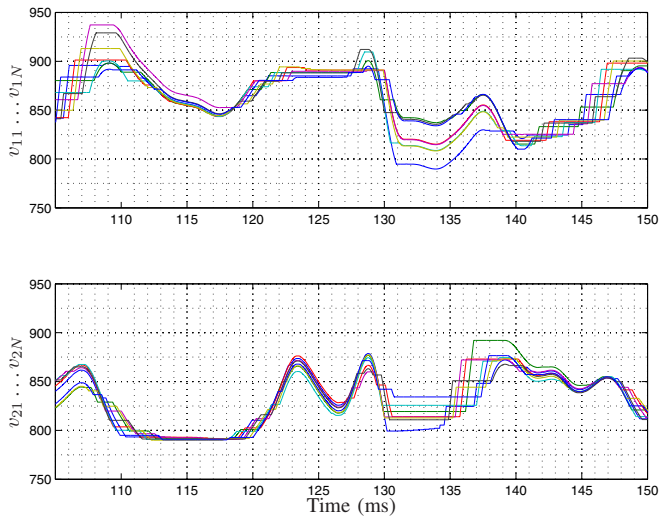


Fig. 10. Capacitor voltages of the N modules of the top and bottom branch, respectively, of the phase leg a during load steps

0.5 ms; to increase the current from zero to rated current takes less than 3 ms, which is an impressive result.

It is also important to note that the capacitor voltages, as shown in Fig. 10, are well balanced throughout the transient events. Due to the inherent ability of MPC to impose and meet constraints on variables, the capacitor voltages are kept within their given bounds even during these relatively extreme transient events, not exceeding their safe operating limits. In fact, the maximum and minimum values of the capacitor voltages during the transients are comparable to the ones at steady-state operation.

The ability of the MPCC scheme to respect the constraints is also visible when analyzing the branch currents, which are shown in Fig. 11 during the transients. It can be seen that the controller effectively "clamps" the branch current to 1.1 p.u. during parts of the transient. This is a significant achievement

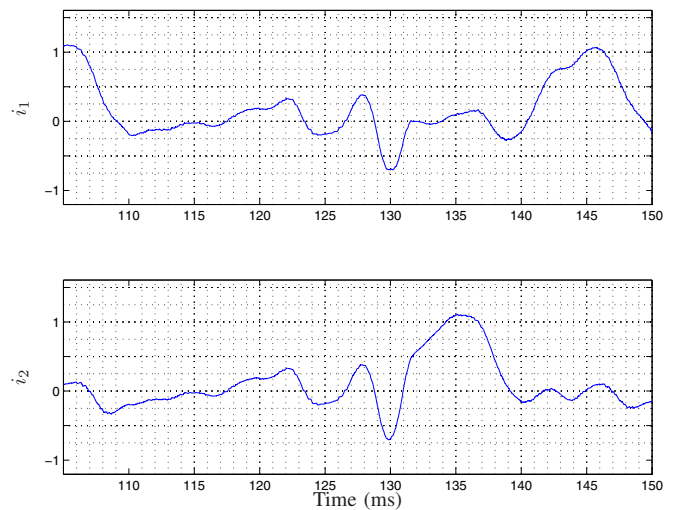


Fig. 11. Branch current of the top and bottom branch, respectively, of the phase leg a during load steps

by the controller, since the second-order energy exchange between the branch inductors and module capacitors must be controlled in a considerate manner to avoid any overshoot in the capacitor voltages and branch currents.

V. CONCLUSIONS

A model predictive current control (MPCC) scheme with a PWM was proposed in this paper for the MMC topology. This versatile control approach is applicable to any MMC regardless of its circuit parameters, phase configuration and number of modules. The controller is conceptually simple with an easy to devise objective function, a linearized converter model based on first principles and constraints on the main physical quantities. The underlying optimization problem is a quadratic program (QP), which can be solved efficiently using off-the-shelf solvers. Unlike traditional control schemes with multiple PI loops, the design effort is low, but the computational effort is relatively high, requiring a dedicated QP solver running on a DSP or FPGA.

Due to its ability to address the MMC as a multiple-input multiple-output (MIMO) problem with operating constraints, MPCC outperforms most of the existing control approaches for the MMC, particularly during transients. Very fast responses close to the physical limits of the MMC are achieved. Overshoots in the capacitor voltages and the branch currents are avoided, and the operation of the converter within safe operating limits is ensured under all circumstances. At steady-state operation, a very low current THD of about 0.5% is achieved, while operating the IGBTs at a low switching frequency of less than 400 Hz.

VI. APPENDIX

The time-varying matrices and vectors $A_c(t_0)$, $B_c(t_0)$, $f_c(t_0)$ and C_c of the linearized continuous-time state-space

model (7) are given by

$$A_c(t_0) = \begin{bmatrix} A_{11} & A_{12} & A_{13} \\ A_{21} & A_{22} & A_{23} \\ A_{31} & A_{32} & A_{33} \end{bmatrix} \quad B_c(t_0) = \begin{bmatrix} B_1 \\ B_2 \\ B_3 \end{bmatrix}$$

$$f_c(t_0) = \begin{bmatrix} f_1 \\ f_2 \\ f_3 \end{bmatrix} \quad C_c = \begin{bmatrix} C_1 & C_2 & C_3 \end{bmatrix}$$

where

$$A_{11} = T^{-1}F, \quad A_{12} = T^{-1}M, \quad A_{13} = T^{-1}HK$$

$$A_{21} = \frac{N}{C_m} \begin{bmatrix} n_1(t_0) & 0 & 0 & 0 & 0 \\ 0 & n_2(t_0) & 0 & 0 & 0 \\ 0 & 0 & n_3(t_0) & 0 & 0 \\ 0 & 0 & 0 & n_4(t_0) & 0 \\ -n_5(t_0) & 0 & -n_5(t_0) & 0 & n_5(t_0) \\ 0 & -n_6(t_0) & 0 & -n_6(t_0) & n_6(t_0) \end{bmatrix}$$

$$A_{22} = 0_{6 \times 6}, \quad A_{23} = 0_{6 \times 2}, \quad A_{31} = 0_{2 \times 5}$$

$$A_{32} = 0_{2 \times 6}, \quad A_{33} = \omega \begin{bmatrix} 0 & -1 \\ 1 & 0 \end{bmatrix}$$

$$B_1 = T^{-1}G$$

$$B_2 = \frac{N}{C_m} \text{diag}(i_1(t_0) \ i_2(t_0) \ i_3(t_0) \ i_4(t_0) \ i_5(t_0) \ i_6(t_0)), \quad B_3 = 0_{2 \times 6}$$

$$i_5(t_0) = (i_{dc}(t_0) - i_1(t_0) - i_3(t_0)), \quad i_6(t_0) = (i_{dc}(t_0) - i_2(t_0) - i_4(t_0))$$

$$f_1 = T^{-1}\Lambda, \quad f_2 = 0_{6 \times 1}, \quad f_3 = 0_{2 \times 1}$$

$$C_1 = \begin{bmatrix} C_{11} \\ C_{12} \end{bmatrix}, \quad C_2 = \begin{bmatrix} C_{21} \\ C_{22} \end{bmatrix}, \quad C_3 = \begin{bmatrix} C_{31} \\ C_{32} \end{bmatrix}$$

$$C_{11} = K_i \begin{bmatrix} 1 & -1 & 0 & 0 & 0 \\ 0 & 0 & 1 & -1 & 0 \\ -1 & 1 & -1 & 1 & 0 \end{bmatrix}, \quad C_{12} = 0_{6 \times 5}$$

$$C_{21} = 0_{2 \times 6}, \quad C_{22} = \mathbb{I}_{6 \times 6}$$

$$C_{31} = 0_{2 \times 2}, \quad C_{32} = 0_{6 \times 2}$$

$$K_i = \frac{2}{3} \begin{bmatrix} 1 & -\frac{1}{2} & -\frac{1}{2} \\ 0 & \frac{\sqrt{3}}{2} & -\frac{\sqrt{3}}{2} \end{bmatrix}$$

$$T = \begin{bmatrix} L & L & 0 & 0 & L_{dc} \\ 0 & 0 & L & L & L_{dc} \\ -L & -L & -L & -L & L_{dc} + 2L \\ L_g & -(L + L_g) & -L_g & L + L_g & 0 \\ 2L_g & -2(L + L_g) & L_g & -(L + L_g) & L \end{bmatrix}$$

$$G = \begin{bmatrix} -v_1^\Sigma(t_0) & -v_2^\Sigma(t_0) & 0 & 0 & 0 & 0 \\ 0 & 0 & -v_3^\Sigma(t_0) & -v_4^\Sigma(t_0) & 0 & 0 \\ 0 & 0 & 0 & 0 & -v_5^\Sigma(t_0) & -v_6^\Sigma(t_0) \\ 0 & v_2^\Sigma(t_0) & 0 & -v_4^\Sigma(t_0) & 0 & 0 \\ 0 & v_2^\Sigma(t_0) & 0 & 0 & 0 & -v_6^\Sigma(t_0) \end{bmatrix}$$

$$M = \begin{bmatrix} -n_1(t_0) & -n_2(t_0) & 0 & 0 & 0 & 0 \\ 0 & 0 & -n_3(t_0) & -n_4(t_0) & 0 & 0 \\ 0 & 0 & 0 & 0 & -n_5(t_0) & -n_6(t_0) \\ 0 & n_2(t_0) & 0 & -n_4(t_0) & 0 & 0 \\ 0 & n_2(t_0) & 0 & 0 & 0 & -n_6(t_0) \end{bmatrix}$$

$$F = \begin{bmatrix} -R & -R & 0 & 0 & -R_{dc} \\ 0 & 0 & -R & -R & -R_{dc} \\ R & R & R & R & -(R_{dc} + 2R) \\ -R_g & R + R_g & R_g & -(R + R_g) & 0 \\ -2R_g & 2(R + R_g) & -R_g & R + R_g & -R \end{bmatrix}$$

$$H = \begin{bmatrix} 0 & 0 & 0 \\ 0 & 0 & 0 \\ 0 & 0 & 0 \\ -1 & 1 & 0 \\ -1 & 0 & 1 \end{bmatrix}, \quad K = \begin{bmatrix} 1 & 0 \\ -\frac{1}{2} & \frac{\sqrt{3}}{2} \\ -\frac{1}{2} & -\frac{\sqrt{3}}{2} \end{bmatrix}, \quad \Lambda = \begin{bmatrix} V_{dc} \\ V_{dc} \\ V_{dc} \\ 0 \\ 0 \end{bmatrix}$$

REFERENCES

- [1] A. Lesnicar and R. Marquardt. An innovative modular multilevel converter topology suitable for a wide power range. In *Proc. IEEE Power Tech. Conf.*, Bologna, Italy, Jun. 2003.
- [2] A. Antonopoulos, L. Angquist, and H. P. Nee. On dynamics and voltage control of the modular multilevel converter. In *Proc. Eur. Conf. on Power Electron. and Applicat.*, 2009.
- [3] M. Hagiwara and H. Akagi. Control and experiment of pulsewidth-modulated modular multilevel converters. *IEEE Trans. Power Electron.*, 24(7):1737–1746, Jul. 2009.
- [4] L. Angquist, A. Antonopoulos, D. Siemaszko, K. Ilves, M. Vasiladiotis, and H.-P. Nee. Inner control of modular multilevel converters — an approach using open-loop estimation of stored energy. In *Int. Power Electron. Conf.*, pages 1579–1585, Jun. 2010.
- [5] A.J. Korn, M. Winkelnkemper, P. Steimer, and J.W. Kolar. Capacitor voltage balancing in modular multilevel converters. In *Proc. 6th IET Int. Power Electron., Machines and Drives Conf.*, pages 1–5, 2012.
- [6] J. B. Rawlings and D. Q. Mayne. *Model predictive control: Theory and design*. Nob Hill Publ., Madison, WI, USA, 2009.
- [7] J.M. Maciejowski. *Predictive control with constraints*. Prentice-Hall, 2002.
- [8] M.A. Pérez, J. Rodríguez, E.J. Fuentes, and F. Kammerer. Predictive control of AC-AC modular multilevel converters. *IEEE Trans. Ind. Electron.*, 59(7):2832–2839, Jul. 2012.
- [9] J. Qin and M. Saeedifard. Predictive control of a modular multilevel converter for a back-to-back HVDC system. *IEEE Trans. Power Deliv.*, 27(3):1538–1547, Jul. 2012.
- [10] B.S. Riar, T. Geyer, and U.K. Madawala. Model predictive direct current control of modular multi-level converters. In *Proc. IEEE Int. Conf. Ind. Technol.*, Cape Town, South Africa, Feb. 2013.
- [11] B. Riar, T. Geyer, and U. Madawala. Model predictive direct current control of modular multilevel converters: Modelling, analysis and experimental evaluation. *IEEE Trans. Power Electron.*, 2014. early access article.
- [12] K. Ilves, A. Antonopoulos, S. Norrga, and H. P. Nee. Steady-state analysis of interaction between harmonic components of arm and line quantities of modular multilevel converters. *IEEE Trans. Power Electron.*, 27(1):57–68, 2012.
- [13] G. Carrara, S. Gardella, M. Marchesoni, R. Salutari, and G. Sciutto. A new multilevel PWM method: a theoretical analysis. *IEEE Trans. Power Electron.*, 7(3):497–505, Jul. 1992.
- [14] D. G. Holmes and T. A. Lipo. *Pulse width modulation for power converters: principles and practice*. IEEE Press, 2003.
- [15] M. Herceg, M. Kvasnica, C.N. Jones, and M. Morari. Multi-parametric toolbox 3.0. In *Proc. Eur. Control Conf.*, pages 502–510, Zürich, Switzerland, July 17–19 2013.
- [16] Inc. Gurobi Optimization. Gurobi optimizer reference manual, 2014.